Evaluation of Model-Based Biomimetic Control of Prosthetic Finger Force for Grasp

Qi Luo, Chuanxin M. Niu, *Member, IEEE*, Jiayue Liu, Chih-Hong Chou, Manzhao Hao, and Ning Lan, *Senior Member, IEEE*

***Abstract*— Restoring neuromuscular reflex properties in the control of a prosthetic hand may potentially approach human-level grasp functions in the prosthetic hand. Previous studies have confirmed the feasibility of real-time emulation of a monosynaptic spinal reflex loop for prosthetic control. This study continues to explore how well the biomimetic controller could enable the amputee to perform force-control tasks that required both strength and error-tolerance. The biomimetic controller was programmed on a neuromorphic chip for real-time emulation of reflex. The model-calculated force of finger flexor was used to drive a torque motor, which pulled a tendon that flexed prosthetic fingers. Force control ability was evaluated in a "press-without-break" task, which required participants to press a force transducer toward a target level, but never exceeding a breakage threshold. The same task was tested either with the index finger or the full hand; the performance of the biomimetic controller was compared to a proportional linear feedback (PLF) controller, and the contralateral normal hand. Data from finger pressing task in 5 amputees showed that the biomimetic controller and the PLF controller achieved 95.8% and 66.9% the performance of contralateral finger in success rate; 50.0% and 25.1% in stability of force control; 59.9% and 42.8% in information throughput; and 51.5% and 38.4% in completion time. The biomimetic controller outperformed the PLF controller in all performance indices. Similar trends were observed with full-hand grasp task. The biomimetic controller exhibited capacity and behavior closer to contralateral normal hand. Results suggest that incorporating neuromuscular reflex properties in the biomimetic controller may provide human-like capacity of force regulation, which may enhance motor performance of amputees operating a tendon-driven prosthetic hand.**

***Index Terms*— Biomimetic control, neuromuscular reflex, neuromorphic computing, prosthetic hand, electromyography (EMG).**

Manuscript received April 1, 2021; revised July 4, 2021 and August 13, 2021; accepted August 17, 2021. Date of publication August 20, 2021; date of current version September 1, 2021. This work was supported in part by the National Key Research and Development Program of China through the Ministry of Science and Technology of China under Grant 2017YFA0701103, in part by the Natural Science Foundation of China under Grant 81630050, and in part by the Science and Technology Commission of Shanghai Municipality under Grant 20DZ2220400. *(Corresponding authors: Ning Lan; Chuanxin M. Niu.)*

This work involved human subjects or animals in its research. Approval of all ethical and experimental procedures and protocols was granted by the Ethics Committee of Human and Animal Experiments of the Med-X Research Institute of Shanghai Jiao Tong University.

Qi Luo, Jiayue Liu, Chih-Hong Chou, and Manzhao Hao are with the Laboratory of Neuro-Rehabilitation Engineering, School of Biomedical Engineering, Shanghai Jiao Tong University, Shanghai 200030, China (e-mail: luoqi_ctp@sjtu.edu.cn; liu.jiayue@sjtu.edu.cn; chchou@sjtu.edu.cn; haomzh@sjtu.edu.cn).

Chuanxin M. Niu is with the Laboratory of Neuro-Rehabilitation Engineering, School of Biomedical Engineering, Shanghai Jiao Tong University, Shanghai 200030, China, and also with the Department of Rehabilitation Medicine, Ruijin Hospital, Shanghai Jiao Tong University, Shanghai 200025, China (e-mail: minos.niu@gmail.com).

Ning Lan is with the Laboratory of Neuro-Rehabilitation Engineering, School of Biomedical Engineering, Shanghai Jiao Tong University, Shanghai 200030, China, and also with the Institute of Medical Robotics, Shanghai Jiao Tong University, Shanghai 200240, China (e-mail: ninglan@sjtu.edu.cn).

Digital Object Identifier 10.1109/TNSRE.2021.3106304

I. Introduction

UPPER-LIMB prostheses have made significant progress in both research and commercial applications [1]–[3]. However, the performance of prosthetic hands are still far from that of human hand, thus prosthetic hands are frequently abandoned or rejected by amputees [4], [5]. Lack of tactile sensation has been identified as one of the major hindrances for prosthetic hands [6]. Another issue is that the control mechanism of prosthesis fundamentally differs from that of human hand, and therefore prosthetic hands cannot faithfully reify the motor intention of amputees [7], [8]. The discrepancy between the motor intention and the actual movement is also prominent in quasi-static tasks of movement, e.g. posture maintenance [9] or object grasping [10]. In these tasks, the focus of motor control lies in the regulation of muscle force [11], [12] rather than movement kinematics. For restoration of hand function, therefore, prosthetic hands must confront the very challenge of force control, especially when coordinated force is required.

However, it is not straightforward for prosthetic hands to replicate human-like force control, especially when the hand has to interact with objects [12], [13]. A major challenge arises from the lack of human-like biomechanical and neurophysiological properties in prosthetic control. In particular, it has been suggested that without neuromuscular apparatus (e.g. viscoelasticity of skeletal muscle [14]) or spinal-level neural circuitry (e.g. dynamics of muscle spindle [15]), it prevents reflexive changes in muscle activation to counteract external perturbations [16], [17]. As a result, amputees operating on a reflex-deprived prosthesis would bound for frustration, because the prosthesis would behave incompatibly with the consequent execution of motor commands [18], and loss of force adjustment via spinal pathways [19].

Computational models of spinal reflex have been developed to prove the role of reflex in reaching [20] and holding [21]. On top of that, reflex-model-based prosthetic control has been attempted with success using neuromorphic hardware, a VLSI (very-large-scale-integrated-circuit) technology that

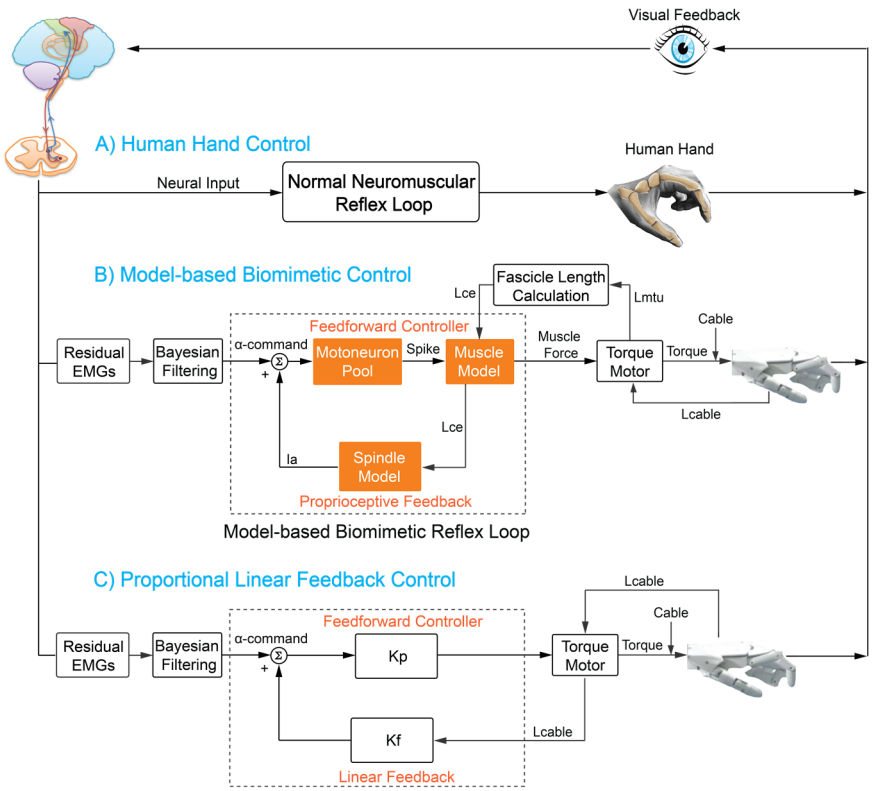

Fig. 1. Control paradigms investigated in this study: A) Human hand control. B) Model-based biomimetic control. C) Proportional linear feedback control.

leads to real-time computation of the reflex model [1]. On the neuromorphic hardware, it has been shown that proprio-motor signals can be engineered into biomimetic forms, i.e., spike trains [22]. Therefore, a reflex-model-based controller for hand prosthesis enables human-like capacity, which originally takes place in the spinal circuitry. Our pilot study has suggested the potential of mode-based controller for mimicking human hand control [1], which may lead to a unique approach for prosthetic control [23] among many other strategies [24]–[29].

In the present study, we assessed the real-time performance of force control by the biomimetic controller driving a cable-powered prosthetic hand. Prosthetic performances were compared to a proportional linear feedback (PLF) controller and the contralateral normal hand of the amputees. The precision and sensitivity of the force control were evaluated in a "press-without-break" task, which required the subject to press or grip a sensorized object with an expected range of force. Based on the same biomimetic controller [1], this paper refined the procedure of coupling between model and prosthetic hand in real-world. We hypothesized that the biomimetic controller may facilitate amputees for force control in the "press-without-break" task with human operations. Some preliminary results were presented in a conference proceeding [30].

II. Material and Methods

Our proposed biomimetic controller was compared to the human hand control in a force control task. Fig. 1A illustrates the neuromuscular reflex control of the human hand. Since the supraspinal structures of amputees are not damaged by amputation, we focus on modeling the spinal level of human nervous system. In a typical joint (e.g. the metacarpophalangeal joint) rotated by an antagonistic pair of muscles, muscle contraction produces the necessary force transferred via tendons that eventually attach to the joint.

A. The Model-Based Biomimetic Controller for Prosthetic Hand

The model-based biomimetic control schematic is shown in Fig. 1B. The biomimetic controller included a virtual motoneuron pool, a virtual skeletal muscle and a virtual muscle spindle, constituting a virtual spinal reflex loop. Alpha motor command was at the entrance to the biomimetic controller. sEMG of wrist flexor was filtered into the alpha motor command and scaled to 0 – 1 by adopting a nonlinear Bayesian algorithm (drift term: $\alpha = 1e-4$; jumping term: ß $= 1e-18$; 128-level quantization) that had proven its advantage in myoelectric control applications [31]. The motor command entered the biomimetic reflex loop activating the motoneuron pool, which was then converted into a muscle force of contraction through muscle model; meanwhile, the calculation of muscle force is constantly adjusted by a biomimetic spindle. Therefore, the monosynaptic spinal loop formed a closed loop for regulating muscle tone and reflex. The model-calculated force of flexor was used to drive a torque motor, which pulled a tendon that flexes prosthetic fingers.

The biomimetic controller was programmed on a neuromorphic chip, which operated a biologically realistic model of neuromuscular reflex in real time. The model included 6 motoneuron pools with 768 spiking neurons, 6 Hill-type muscle fibers, and 1 muscle spindle projecting 128 spiking

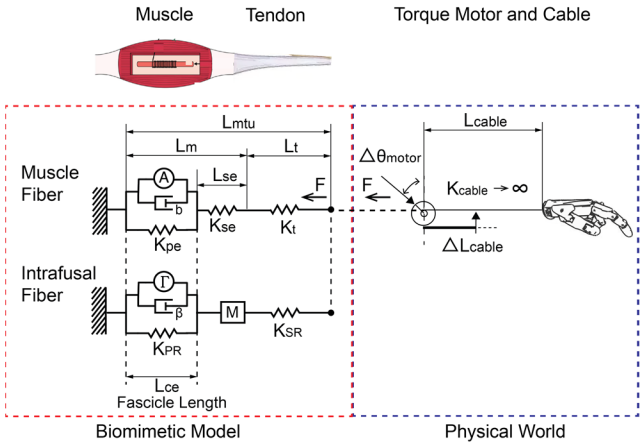

Fig. 2. Muscle length information in the biomimetic muscle model and the interaction with the physical world. Red-dotted region shows the constraint relationship of the key length variables in biomimetic muscle model. Blue- dotted region displays conversion of finger flexion to muscle length. The model-produced force is established by torque motor. The rotation of torque motor ($\Delta\theta_{motor}$) produces a translational movement on the cable (ΔL_{cable}), which opens/closes the prosthetic hand.

Ia afferents. The main control loop of the prosthetic hand was coordinated on a PC (Intel Core i7-8700CPU, 3.20 GHz, 16 GB Memory, Microsoft Windows 10 64-bit) at 100 Hz sampling rate.

B. Proportional Linear Feedback (PLF) Controller

As shown in Fig. 1C, the PLF controller was established for comparison with the BC. Closed-loop control was achieved by superimposing the alpha motor command and a linear feedback. For both the PLF and BC, the feedback gain was set such that 10% of maximum voluntary contraction (MVC) elicited approximately 1% change in the motor command. The linear feedback that converted the length change of driven-cable to motor command, and the length change is measured by a rotational transducer on the torque motor.

C. Tuning the Range of Fascicle Length for Biomimetic Controller

As shown in Fig. 2, the muscle length (L_m) and fascicle length (length of contractile element, L_{ce}) are the key inputs to the muscle model and spindle model, respectively [1]. The length of musculotendinous unit (L_{mtu}) refers to the sum of L_m and the length of tendon (L_t). L_m refers to the sum of L_{ce} and the length of serial elastic element (L_{se}).

The stiffness of cable (K_{cable}) is assumed to be infinite, so that the change in the cable length (ΔL_{cable}) is equivalent to the change in the length of musculotendinous unit (ΔL_{mtu}) in the muscle model. The translational displacement of the cable (ΔL_{cable}) can be measured by a rotational transducer on the torque motor ($\Delta\theta_{motor}$). K_{pe} is the stiffness of the parallel elastic component ($K_{pe} = 0.74$ N/cm) [32], K_{se} is the stiffness of the serial elastic element ($K_{se} = 1.33$ N/cm) [32], and K_t is the stiffness of tendon ($K_t = 1400$ N/cm) [33]. By ignoring the effect of K_t, ΔL_{mtu} can be approximated by ΔL_m. The

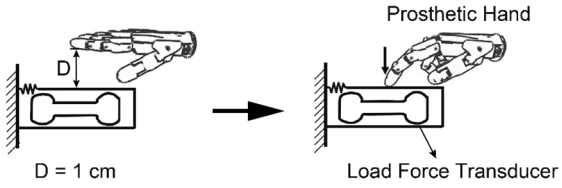

Fig. 3. Experimental setup of force generation test. The prosthetic hand was fully extended at the beginning. A step alpha command was issued to the biomimetic controller, which drove the prosthetic finger to move till the fingertip contact the force transducer.

calculation of fascicle length is given by:

$$L_{ce}(t) = L_{ce}(0) - \Delta L_{ce} \tag{1}$$

$$\Delta L_{ce} = \frac{K_{se}}{K_{se} + K_{pe} + K_{\alpha}} * \Delta L_{mtu} \tag{2}$$

$$K_{\alpha} = \begin{cases} (-57.76\alpha + 60.24) * L_m \\ +57.41\alpha - 12.28, & L_m \le L_m^0 \\ (-14.61\alpha + 15.23) * L_m \\ +14.47\alpha - 32.31, & L_m > L_m^0 \end{cases} \tag{3}$$

where $L_{ce}(t)$ is the instantaneous fascicle length, $L_{ce}(0)$ is its initial value, and ΔL_{ce} is the change in length, α is the alpha motor command. The active component in muscle model is the equivalent of a spring with adjustable stiffness K_{α}, which is inferred from the force-length relationship. The detailed calculation of key variables has been described in a recent study [1].

1) Ranges of Fascicle Length: In the biomimetic controller, the fascicle length played an important role for reflex: it was the source of proprioception that should be explicitly provided to the muscle spindle [15], and the fascicle length must be accessible by the muscle model to engage force-length property [34]. The exact range of fascicle length, however, was unclear from literature. Therefore the range of fascicle range needed to be pre-allocated in order to produce a feasible muscle force.

The previous study allocated a range of 0.5 – 1.6 L_o to the fascicle length, which corresponded to 0° – 60° rotation of metacarpophalangeal (MCP) joint, and 0 – 1.6 cm translational displacement in the cable [1]. L_o was the optimal length for force production at which active muscle force peak (standard value of normalized muscle length) [34], [35]. The range of 0.5 – 1.6 L_o centered around L_o, which was close to the maximal range supported by previous experiments [34]. However, this range contributed a negative component to the overall muscle stiffness [34], which might reduce the capacity of force generation. Therefore, two ranges of fascicle length (R_1: 0.5 – 1.0 L_o; R_2: 0.5 – 1.6 L_o) were proposed. R_1 only worked in the positive stiffness zone of the active component of muscle; R_2 included both positive and negative muscle stiffness regions.

2) Force Generation With Different Ranges of Fascicle Length: Capability of force generation was tested using a finger-pressing task. The index finger of the prosthetic hand was activated to press down a force transducer (Model FNA, 0 – 30 N, Forsentek Co., Ltd., Shenzhen, China), which recorded the downward pressure (fingertip force) at 100 Hz

TABLE I
CLINICAL INFORMATION OF AMPUTEES

Participant	Age	Sex	Amputation level and side	Years since amputation	Ever used myoelectric prosthesis?
S1	65	M	Left Distal third of left forearm (long residual limb)	15	Yes
S2	50	M	Left Distal third of left forearm (long residual limb)	35	None
S3	39	M	Right Distal third of right forearm (middle residual limb)	15	Yes
S4	45	F	Right Distal third of right forearm (long residual limb)	6	None
S5	65	M	Left Distal third of left forearm (long residual limb)	42	None

with 12bit resolution (Model USB-201, Measurement Computing Corp., MA, U.S.). As shown in Fig. 3, the prosthetic finger was initially hovering at 1 cm above the force transducer (D = 1cm). Thereafter, a step alpha command was issued to the biomimetic controller, which drove the prosthetic finger to move till the fingertip contact the force transducer. Since the load force transducer was deformable, five events should occur in series during pressing: change in torque, change in fascicle length, contact of object, end of deformation, settlement of force. A cable-driven prosthetic hand controlled by the biomimetic model could reproduce all 5 events in the correct order [1].

Between R_1 and R_2, our human experiment proceeded with the range that generated larger maximal force in the above test.

D. Participant Details

Five forearm amputees (one female, four males, age range: 39 – 65 years) participated in the study. The detailed descriptions of amputees are listed in Table I. All participants had 10 cm to 18 cm left in the forearm stump, leaving their FCU muscles all functioning, and they reported having no cognitive disabilities, had normal or corrected-to-normal vision. This study was approved by the Ethics Committee of Human and Animal Experiments of the Med-X Research Institute of Shanghai Jiao Tong University. All participants gave written consent before joining the study.

E. Experimental Setup

In the human-in-the-loop experiments, each participant sat in a chair in front of a computer screen, placed about 60 cm from the participant (Fig. 4). The raw surface EMG signals were sampled at rate of 1962 Hz by Delsys system (Trigno™Wireless EMG System, Delsys Inc., US) from flexor carpi ulnaris (FCU). FCU was chosen because this muscle was still functioning after forearm amputation, and FCU could easily be recorded using sEMG for myocontrol [28], [36], [37]. A cable-driven prosthetic hand was used in the experiments, which was favored for biomimetic control. The detailed design of the prosthetic hand device had been described in previous

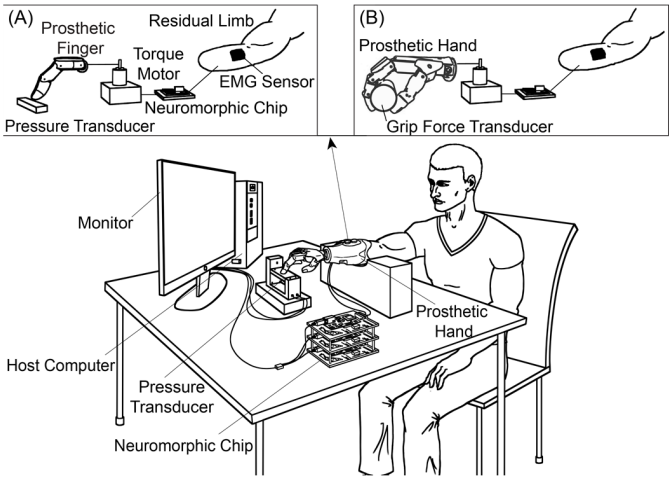

Fig. 4. Human experiment for force control. (A) Single-finger experiment. At the beginning of each trial, the index finger stayed at a default position 1cm above the pressure transducer, meaning that the finger needed to move through the 1cm distance, contact the transducer, and control the pressure to meet the requirements for task completion. (B) Full-hand experiment. At the beginning of each trial, the prosthetic hand stayed at a default position 35 mm above the grip force transducer, which ensured that the thumb and other fingers hold the middle position of the grip force transducer. A host computer coordinated the experiment for acquisition of EMG, filtering of the alpha motor command from EMG, interaction with neuromorphic models, and transmission of calculated commands to the torque motor. Subjects were free to look at either the screen or the prosthetic hand during experiment.

work [1]. Each amputee accomplished the tasks with the stump resting inside the socket of the prosthetic hand. The socket was mounted and fixed to the table (Fig. 4).

For the single-finger experiment, the index finger of the prosthetic hand pressed a load force transducer (Model FNA, 0 – 30 N, Forsentek Co., Ltd., Shenzhen, China), which recorded the downward pressure at 100 Hz with 12-bit resolution (Model USB-201, Measurement Computing Corp., MA, U.S.). For the full-hand experiment, the prosthetic hand grasped a cylindrical grip force transducer (Model FFK, 0 – 100 N, Forsentek Co., Ltd., Shenzhen, China), which recorded the grip force at 100 Hz with 12-bit resolution (Model USB-201, Measurement Computing Corp., MA, U.S.). Visualization and data collection were developed using Unity 3D (version 2017, Unity Technologies, CA).

F. Experimental Protocols

Each amputee participated in two experiments: (1) Single-finger experiment; (2) Full-hand experiment. Each experiment took approximately two hours. In order to avoid fatigue, all 5 participants accomplished the experiments in two separate visits. It was always the case that the first visit was single-finger experiment, and the second visit was full-hand experiment. About 20 minutes of familiarization were given to each participant prior to the experiments within the same visit. Within each visit, both the types of controller and trials with various Indices of Difficulty (defined below) were randomized.

The detailed experimental design is as follows:

1) Single-Finger Experiment: Subjects were instructed to accomplish a series of "press-without-break" tasks by controlling the pressure with the index finger. The monitor displayed

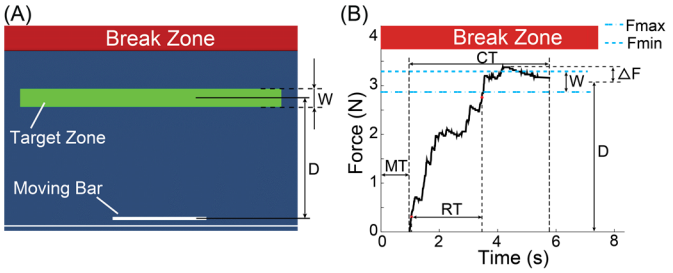

Fig. 5. A) The display during a typical "press-without-break" trial; The height of the white moving bar was linked to the fingertip force. The goal of the task was to escalate the moving bar and stay in the green target zone for 1 second. Task difficulty increases with longer distance (D) and narrower width (W). Red break zone indicates object breakage. B) A representative trial of success in the experiment. From movement onset (t = 0), the subject took MT seconds to move till the fingertip contacted the transducer. From the moment of reaching 10% target force, the subject took RT seconds to move till 90% target force. From the time of contact (t = MT), the subject took CT seconds to stabilize the force within (F_{min}, F_{max}) for 1 second. ΔF is the amount of force exceeding the target level.

a moving bar, whose height indicated the magnitude of the transducer force. In each trial, the subject was requested to escalate the moving bar as quickly as possible to a green target zone, which was achieved by contracting the FCU muscle to flex the prosthetic finger (Fig. 4A). At the beginning of each trial, the finger stayed at a default position 1cm above the force transducer, meaning that the finger needed to move through the 1cm distance, contact the transducer, and control the force to meet the requirements for task completion.

A trial was considered successful once the moving bar had stayed in the target zone for 1 second (dwelling time = 1 s). Above the target zone there was a break zone in red (Fig. 5A), subjects were informed that entering the break zone meant breaking the virtual object, which should be avoided at all times. We chose a breakage threshold (lower bound of break zone) of 4.4 N in this experiment. The breakage threshold was set at about 30% larger than the upper bound of the highest target zone. A failed trial was recorded either when the trial expired at 15 seconds, or when object breakage was detected. The time profile of a successful trial is shown in Fig. 5B. In general, the "press-without-break" task was introduced to test whether an expected force can be produced quickly and accurately, under the restriction of object brittleness. Visual feedback was constantly available to subjects.

2) Full-Hand Experiment: Subjects also were instructed to accomplish a series of "press -without-break" tasks by controlling full-hand gripping. The requirements are similar as in the single-finger experiment. In each trial, the subject was requested to escalate the moving bar to a green target zone as quickly as possible (Fig. 4B). At the beginning of each trial, the prosthetic hand stayed at a default position 35 mm above the grip force transducer, which ensured that the thumb and other fingers hold the middle position of the grip force transducer when the prosthetic hand grasped it. The break zone had a breakage threshold of 8.5 N in this experiment that was also about 30% larger than the upper bound of the highest target zone. Visual feedback was available to participants at all times.

TABLE II
LIST OF DISTANCES (D) AND WIDTHS (W) AND THE CORRESPONDING INDICES OF DIFFICULTY (ID)

(A) Single-finger experiment			(B) Full-hand experiment		
D (N)	W (N)	ID (bits)	D (N)	W (N)	ID (bits)
1.8	0.1	5.17	3.6	0.2	5.17
1.8	0.2	4.17	3.6	0.4	4.17
1.8	0.3	3.59	3.6	0.6	3.59
3.1	0.1	5.95	6.2	0.2	5.95
3.1	0.2	4.95	6.2	0.4	4.95
3.1	0.3	4.37	6.2	0.6	4.37

For both the single-finger and full-hand experiments, each trial is associated with an Index of Difficulty (ID), formulated as $ID = log_2(2D/W)$ [38]. According to Fitts' Law [38], the performance of task is characterized by the relationship between ID and Completion Time (CT, the duration for task completion). A total of 6 different IDs were set in the experiment. Table II shows the target distances (D) and target width (W) corresponding to each ID in single-finger and full-hand experiments.

Either the single-finger or the full-hand experiment consisted of 144 trials, divided into 3 blocks: Block 1 (PLF controller); Block 2 (biomimetic controller); Block 3 (contralateral normal hand). In each block, the subject performed 48 trials (6 IDs and 8 repetitions of each). There was a five-minute break between adjacent blocks, and adhoc breaks were allowed at any time the subject wanted to rest.

G. Performance Metrics and Data Processing

In order to quantify the performance of the prosthetic hand in the force control task, the following outcome metrics were assessed:

1) Success and Breakage Metrics: Each trial can be assessed with a binomial outcome of Success (0-Failed, 1-Succeeded), and a binomial outcome of Break (0-Never entered the break zone, 1-Entered the break zone/Object broken).

2) Performance Metrics: a) RT (Rise Time) is the time required for the force response to rise from 10% to 90% of the target force. In specific, we focused on the variability of RT across different Indexes of Difficulty, measured in standard deviation:

$$Stdev(RT) = \sqrt{\frac{1}{N-1}\sum_{i=1}^{n}\sum_{j=1}^{m}\left(RT_{i,j} - \overline{RT}\right)^2} \quad (4)$$

where $RT_{i,j}$ is the rise time of the ith trial under the jth ID, $\overline{RT}$ is the average of N rise times, m is the number of IDs, n is the number of repetitions for each ID, N is equal to n times m ($N = n \times m$).

b) OS (Overshoot) is the percentage of the magnitude of the force response exceeding the target force. Similar to RT, we focused on the variability of OS across different Indexes of Difficulty, defined as follows:

$$Stdev(OS) = \sqrt{\frac{1}{N-1}\sum_{i=1}^{n}\sum_{j=1}^{m}\left(OS_{i,j} - \overline{OS}\right)^2} \quad (5)$$

TABLE III
THE MAXIMUM FORCE PRODUCED BY AMPUTEE'S CONTRALATERAL HAND WITH THE INDEX FINGER PRESSING A LOAD FORCE TRANSDUCER (A) OR FULL-HAND GRASPING A GRIP FORCE TRANSDUCER (B)

Subject	(A) Force produced of one finger at 100% MVC	(B) Force produced of full-hand grip at 100% MVC
S1	20.7 N	58.3 N
S2	22.0 N	53.5 N
S3	25.7 N	55.5 N
S4	19.9 N	52.3 N
S5	22.6 N	53.1 N

where $OS_{i,j}$ is the overshoot of the ith trial under the jth ID, $\overline{OS}$ is the average of N overshoots, m is the number of IDs, n is the number of repetitions for each ID, N is equal to n times m ($N = n \times m$).

c) Throughput (TP) is a measure for the rate of information transmission, defined as the ratio between the index of difficulty (ID) and completion time (CT) [38].

In the study, two modifications were added to the formulation of TP. First, since only successful trials could transmit information, TP was multiplied with Success Rate (SR) to penalize the controller that failed more trials.

Second, the 3 controllers differed in their maximum capability of force generation, which made the same ID appeared more difficult if it was more effort-taking. As such, we introduced a calibration factor $CF = F_{MVC_{ch}}/F_{MVC_{bc}}$. ($F_{MVC_{bc}}$ and $F_{MVC_{ch}}$ are the forces produced by the prosthetic hand and the contralateral hand at MVC). Since $F_{MVC_{bc}}$ mainly reflect the maximum torque of our torque motor, $F_{MVC_{bc}}$ remained the same of all amputees (15 N for single-finger pressing, 20 N for full-hand grasp). $F_{MVC_{ch}}$ measured for each amputee is shown in Table III.

With these two modifications, the calibrated ID and TP are as follows:

$$ID_{CF} = log_2(2D * CF/W) \tag{6}$$

$$CTP = SR * \frac{1}{K}\sum_{i=1}^{N} ID_{CF_i}/CT_i \tag{7}$$

where K is the number of IDs, and CT is the time for task completion in each trial.

d) IP (Index of Performance) is a measure for the capability of maintaining speed-accuracy relationship, it is defined as IP = 1/b. b refers to the slope of the linear regression between CT and ID. The larger the value of IP, the less CT is affected by increases in ID [39].

3) Force-Specific Metrics: To further evaluate the control performance of the biomimetic controller, we assessed the force generation and regulation capabilities of the prosthetic hand when interacting with objects.

a) Stability of force control: We adopt FM_{RMSE} to evaluate the stability of force control of the control strategies. It is calculated as follows [40]:

$$FM_{RMSE} = \sqrt{\frac{1}{T}\sum_{t=0}^{t=T}\left(F(t) - \overline{F}\right)^2} \tag{8}$$

where F denotes the applied force of prosthetic hand or amputee's contralateral hand, $\overline{F}$ is the average force across all repetitive trials, and T stands for the force's duration.

b) Similarity of force: The cosine of the angle is used to measure the angle between the two sets of vectors. Each element of the vector is positive, and the range of the cosine of the angle is 0 – 1. The larger the value, the more "similar" the two force vectors are. When the value is 1, the two vectors are identical.

The force similarity (FS) between the force generated by prosthetic hand (F_{BC}) and the contralateral hand (F_{CH}) can be expressed as follows [41]:

$$FS = \cos(F_{BC}, F_{CH}) = \frac{F_{BC} \cdot F_{CH}}{\|F_{BC}\| \cdot \|F_{CH}\|} = \frac{\sum_{t=0}^{t=T} F_{BC}(t) \cdot F_{CH}(t)}{\sqrt[2]{\sum_{t=0}^{t=T} F_{BC}(t)^2 \cdot \sum_{t=0}^{t=T} F_{CH}(t)^2}} \tag{9}$$

where F_{CH} stands for the measured force of amputee's contralateral hand, F_{BC} denotes the applied force of the prosthetic hand, and T stands for the force's duration.

H. Statistical Analysis

We analyzed the results for each performance metric with the linear mixed model [42]. Since the success or failure of one trial was a binomial variable, so we adopted a logistic regression model (Generalized Linear Mixed Model, GLMM) [43] for statistical analysis on the metrics of Success and Break. Mixed effects analyses were conducted with ID (6 levels) and control strategy (3 levels) as fixed effects, allowing subject-specific intercepts as a random effect. The model in R syntax was as follows:

$$Metric \sim Controller + ID + (1 \mid Subject) \tag{10}$$

We further conducted post-hoc comparisons with a Tukey test whenever required. In addition, one-way repeated measures ANOVA was performed to detect the statistical differences in stdev (RT), TP and CTP under different control strategies. Data processing was done using MATLAB (R2014b, MathWorks Inc., Natick, MA). All averages are reported ± standard deviation of the mean (Mean ± SD). All statistical analysis was carried out with R, version 4.1.0, and the R-package lmerTest (version 3.1-3) and stats (version 4.1.0). All statistical and correlation analyses were run with significance as $p < 0.05$.

III. RESULTS

A. Choice of Fascicle Length Based on Force Generation Capability

Fig. 6A and Fig. 6B show the linear relationship between the force generated by the prosthetic finger and alpha motor

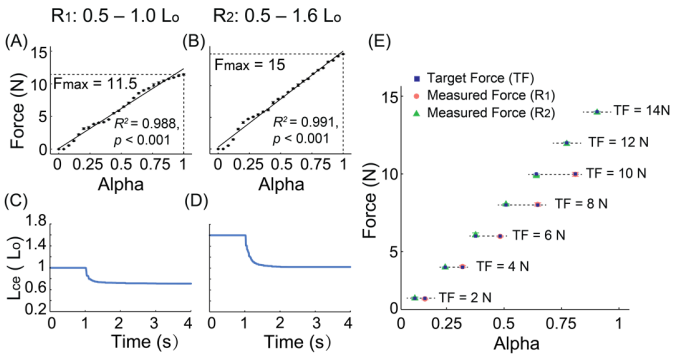

Fig. 6. A) and B) Prosthetic finger generation force in response to alpha motor command in two fascicle length ranges (R_1: 0.5 – 1.0 L_o; R_2: 0.5 – 1.6 L_o); C) and D) Dynamic change of L_{ce} when Alpha = 1; E) Comparison of the ability of prosthetic finger to produce target forces (TF = 2 N, 4 N, 6 N, 8 N, 10 N, 12 N, 14 N) in R_1 and R_2. The target forces (TF = 12 N,14 N) could be generated in R_2, but it could not be achieved in R_1.

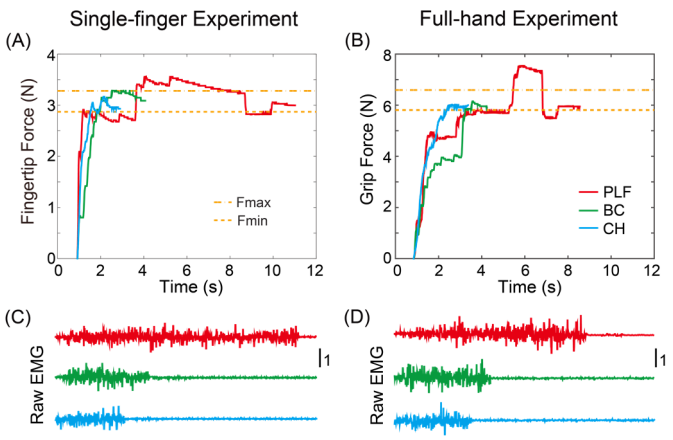

Fig. 7. Time profiles of force and EMGs of one representative trial in each control strategy (PLF, BC, CH) for an amputee (S4). The time responses of force in single-finger experiment (A) and full-hand experiment (B); The raw EMGs recorded in single-finger experiment (C) and full-hand experiment (D).

command in two ranges of fascicle length, averaged across 3 measurements. With R_1, the generated force was approximately 11.43 ± 0.09 N when the alpha motor command reached the maximum value of 1 (Fig. 6A). The linear relationship between the fingertip force and alpha command was significant ($R^2 = 0.989$, $p < 0.001$). Similarly, with R_2, the generated force was about 14.97 ± 0.05 N when the alpha motor command reached the maximum value of 1 (Fig. 6B). The linear relationship between the fingertip force and alpha command was significant ($R^2 = 0.991$, $p < 0.001$). Fig. 6C and Fig. 6D show the dynamic changes of L_{ce} when the alpha motor command reached the maximum value of 1 in two L_{ce} ranges. With R_1, L_{ce} changed from the initial value 1.0 L_o to about 0.75 L_o. And with R_2, L_{ce} changed from the initial value 1.6 L_o to about 1.02 L_o.

Fig. 6E shows the ability of prosthetic finger to produce target forces in R_1 and R_2, averaged across 3 measurements. The average relative error between the generated force and the target force is 1.34 % in R_1 and 1.26 % in R_2. The prosthetic finger could produce greater target force in R_2 compared to in R_1. The target forces (TF = 12 N,14 N) could be generated by prosthetic finger in R_2, but it could not be achieved in R_1. Moreover, when the prosthetic finger produced same target force, the alpha command sent to the controller in R_2 is less than that in R_1. This meant that amputees manipulated the prosthetic hand to produce certain force, which required less muscle contraction in R_2 than in R_1.

Since the prosthetic finger generated larger maximal force in R_2, we proceeded with this range of fascicle length in the ensuing experiments.

B. Characteristics of Force Responses

The time profiles of force of one representative trial for an amputee in each control strategy are shown in Fig. 7. The force generating and regulating patterns were different with the three control strategies. Furthermore, the CH took the least completion time, followed by the BC, and the PLF took the longest time due to trial-and-error force jumps. The difference in kinematics between these two tests (single-finger pressing and full-hand gripping) was likely due to different hand configurations. Raw EMGs recorded from the FCU of the subject are shown in Fig. 7C and Fig. 7D.

C. Single-Finger Experiment

1) Success and Object Breakage: The generalized linear mixed models showed that there was a significant fixed effect of control strategies on the binomial outcomes of Success and Break in the single-finger experiment (Fig. 8A and Fig. 8B). Post-hoc comparisons revealed that Success was significantly increased when using the BC, compared to the PLF ($p < 0.001$). Furthermore, there was no statistically significant difference in Success between the BC and CH ($p = 0.055$). Break was significantly lower when using the BC compared to the PLF ($p < 0.001$). There was no significant difference in Break between the BC and CH ($p = 0.244$).

2) Variability of Rise Time and Overshoot: Control Strategy significantly affected stdev(RT) and stdev(OS) (Fig. 8C and Fig. 8D, stdev(RT): p < 0.001, stdev(OS): p < 0.001). Post-hoc analysis revealed that there was no statistically significant difference in stdev(RT) between the BC and the PLF ($p = 0.375$). And the stdev(RT) with the CH was significantly less than the BC ($p < 0.05$) and the PLF ($p < 0.01$). Furthermore, stdev(OS) was significantly increased when using the PLF compared to the BC ($p < 0.001$) and the CH ($p < 0.001$). There was no statistically significant difference in stdev(OS) between the BC and the CH ($p = 0.173$).

3) Speed and Accuracy Trade-Off: Control Strategy significantly affected TP (Fig. 8E, left panel, $p < 0.001$) and CTP (Fig. 8E, right panel, $p < 0.001$). Post-hoc analysis showed that there was no statistically significant difference in TP between the BC and the PLF ($p = 0.826$). And TP with the CH was significantly higher than the BC ($p < 0.001$) and the PLF ($p < 0.001$). More prominently, CTP with the BC was significantly improved in comparison to that with the PLF ($p < 0.001$). Also, CTP with the CH was significantly higher than the BC ($p < 0.001$). Values of TP of the three control strategies were 1.770 ± 0.646 bits/s (PLF),

1.829 ± 0.305 bits/s (BC) and 3.107 ± 0.270 bits/s (CH). Values of CTP were 1.315 ± 0.516 bits/s (PLF), 1.946 ± 0.393 bits/s (BC) and 3.056 ± 0.318 bits/s (CH).

The linear relationship between CT and ID in the single-finger experiment is shown in Fig. 8F. IP with the CH was highest, followed by the BC, then the PLF ($IP_{PLF} = 0.781$; $IP_{BC} = 1.116$ bits/s; $IP_{CH} = 2.206$ bits/s). Control Strategy showed a significant fixed effect on CT ($p < 0.001$). Post-hoc comparisons revealed that the average CT for all IDs with the BC was significantly less than that with the PLF ($p < 0.001$). And CT was significantly declined when using the CH compared to the BC ($p < 0.001$). Values of CT of the PLF, BC and CH were 4.130 ± 3.015 s, 3.083 ± 1.801 s and 1.587 ± 0.573 s, respectively.

4) Force-Specific Metrics: In the single-finger experiment (Fig. 8G), Control Strategy showed a significant fixed effect on FM_{RMSE} ($p < 0.001$). Post-hoc comparisons revealed that when adopting the BC, FM_{RMSE} significantly decreased compared to the PLF ($p < 0.001$). When using the CH, FM_{RMSE} were significantly lower than the BC ($p < 0.001$). Values of FM_{RMSE} of the three control strategies were 0.794 ± 0.536 (PLF), 0.401 ± 0.385 (BC) and 0.199 ± 0.243 (CH). As shown in Fig. 8H, when adopting the BC, the force similarity (FS) significantly increased in comparison to the PLF ($p < 0.001$).

D. Full-Hand Experiment

1) Success and Object Breakage: The generalized linear mixed model revealed that there was a significant effect of the Control Strategies on the binomial outcomes of Success and Break in the full-hand experiment (Fig. 9A and Fig. 9B). Post-hoc analysis showed that the occurrence of Success was significantly increased when using the BC compared to the PLF ($p < 0.001$). And Success was significantly improved when using the CH compared to the BC ($p < 0.05$). Break was significantly declined when using the BC compared to the PLF ($p < 0.001$). The difference was non-significant in Break between the BC and CH ($p = 0.081$).

2) Variability of Rise Time and Overshoot: Control Strategy showed a significant main effect on stdev (RT) and stdev (OS) (Fig. 9C and Fig. 9D, stdev (RT): $p < 0.001$, stdev (OS): $p < 0.001$). Post-hoc comparisons revealed that there was no significant difference in stdev(RT) between the BC and the PLF ($p = 0.090$). And stdev(RT) with the CH was significantly less than the BC ($p < 0.05$) and PLF ($p < 0.001$). In addition, stdev (OS) with the BC was significantly decreased compared to the PLF ($p < 0.05$). When using the CH, stdev (OS) was less than using the BC ($p < 0.001$) or PLF ($p < 0.001$).

3) Speed and Accuracy Trade-Off: The main effects of Control Strategy were significant on TP (Fig. 9E, left panel, $p < 0.001$) and CTP (Fig. 9E, right panel, $p < 0.001$) in the full-hand experiment. Post-hoc comparisons revealed that TP with the BC was significantly higher than the PLF ($p < 0.001$). And TP with the CH was significantly higher than the BC ($p < 0.001$). Additionally, CTP with the BC was significantly higher than the PLF ($p < 0.001$). Also, CTP with the CH was significantly higher than the BC ($p < 0.01$). Values of TP of the three control strategies were 1.575 ± 0.474 bits/s (PLF), 1.962 ± 0.328 bits/s (BC) and 2.809 ±0.295 bits/s (CH). Values of CTP were 1.440 ± 0.529 bits/s (PLF), 2.409 ± 0.466 bits/s (BC) and 2.764 ± 0.339 bits/s (CH).

The linear relationship between CT and ID in the grip task is shown in Fig. 9F. IP of the CH was higher than that of the BC and PLF ($IP_{PLF} = 1.014$ bits/s; $IP_{BC} = 1.479$ bits/s; $IP_{CH} = 2.222$ bits/s). Control Strategy showed a significant fixed effect on CT ($p < 0.001$). Post-hoc comparisons showed that average CT for all IDs with the BC was significantly less than the PLF ($p < 0.001$). When using the CH, CT was significantly declined compared to the BC ($p < 0.001$). CTs of PLF, BC and CH were 4.310 ± 3.039 s, 2.909 ± 1.669 s and 1.745 ± 0.527 s, respectively.

4) Force-Specific Metrics: In the full-hand experiment (Fig. 9G), Control Strategy showed a significant fixed effect on FM_{RMSE} ($p < 0.001$). Post-hoc comparisons revealed that FM_{RMSE} significantly reduced when the PLF switched to the BC ($p < 0.001$). Compared with using the BC, FM_{RMSE} significantly declined when adopting the CH ($p < 0.001$). Values of FM_{RMSE} of the three control strategies were 1.629 ± 1.048 (PLF), 0.844 ± 0.856 (BC) and 0.379 ± 0.498 (CH). As shown in Fig. 9H, FS significantly increased when the PLF switched to the BC ($p < 0.001$).

IV. Discussion

In this study, we evaluated the force control capability of the biomimetic controller in a cable-powered prosthetic hand. A "press-without-break" task was designed to assess the precision and sensitivity of force control. Using the biomimetic controller, all 5 amputees were able to complete the task, both with an index finger and the full prosthetic hand. Although neither the biomimetic nor the proportional-linear controller could surpass the contralateral hand in task performance, the biomimetic controller reached 95.8% (single-finger) and 94.5% (full-hand) the performance of contralateral hand in success rate. In other aspects of performance, the biomimetic controller achieved no less than 50.6% of the performance of the contralateral hand. Results also showed that the biomimetic controller consistently outperformed the PLF controller in both single-finger and full-hand experiments. Our results supported the hypothesis that the biomimetic control with neuromuscular reflex may offer a novel way of controlling hand prosthesis with human-like behaviors.

Experiments in this study focused on grasping. Successful grasping control satisfying both strength and dexterity can be attributed to several characteristics of the hand. For one thing, the force is programmed and issued by the central nervous system (CNS) [44]; the CNS also regulates the force in a process known as "grip-force/load-force coupling" [45]. For another, sensory signals from the hand are also instrumental, which continuously convey information about the hand gesture and object interaction [46]. Last but not least, the overall force applied from the hand is reconciled among many biomechanical and neurological properties, e.g. the viscoelasticity of muscle [14], the routing of tendon network [47], the moment of

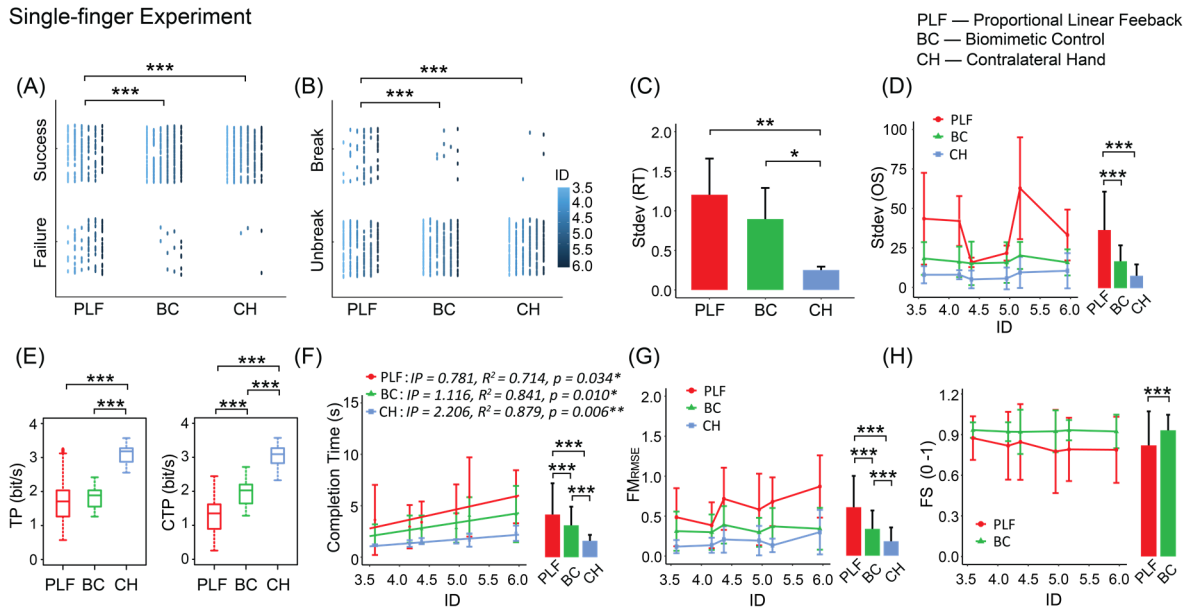

Fig. 8. Performance metrics in the single-finger experiment. A) and B) Binomial outcomes, 720 dots are categorized as success/failure trials (A) or trials with/without breakage (B). Trials are also color-coded to 6 Indexes of Difficulty. Contralateral hand shows the more successful trials and the fewer occurrences of breakage; C) Variability of rise time; D) Variability of overshoot; E) Throughput (left panel) and Calibrated Throughput (right panel); F) shows the linear relationship between completion time (CT) and index of difficulty (ID) and the average completion time; G) shows the force control stability, and the smaller FM_{RMSE}, the higher the stability; H) shows the force similarity (FS) between the force generated by the prosthetic hand and the contralateral hand. (*, $p < 0.05$; **, $p < 0.01$; ***, $p < 0.001$).

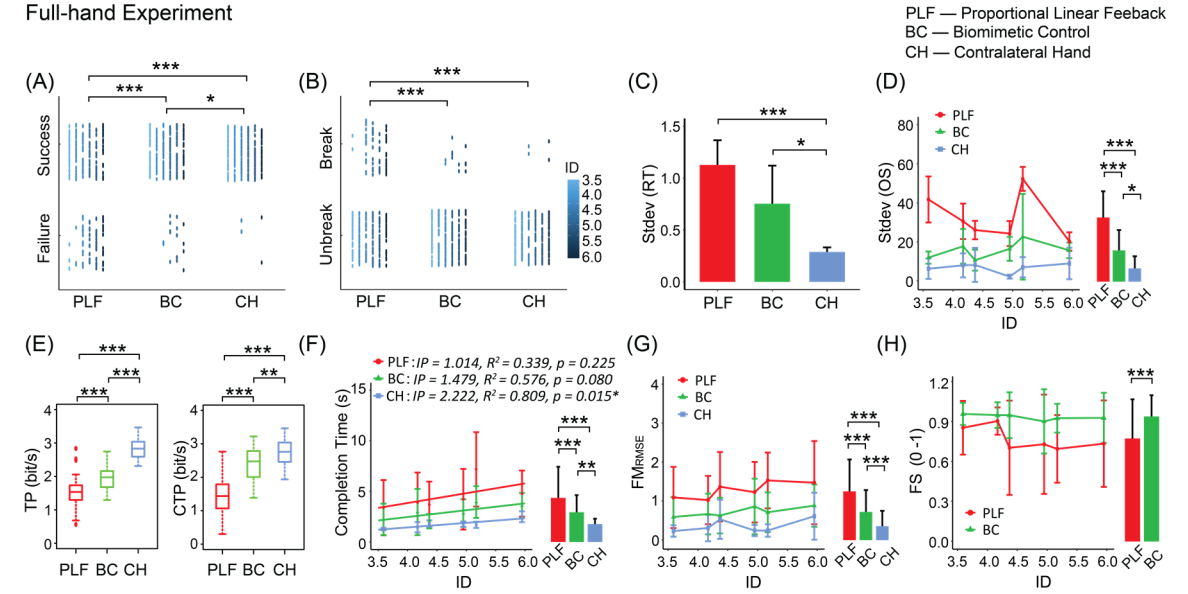

Fig. 9. Performance metrics in the full-hand experiment. A) and B) Binomial outcomes, 720 dots are categorized as success/failure trials (A) or trials with/without breakage (B). Contralateral hand shows the more successful trials and the fewer occurrences of breakage; C) Variability of rise time; D) Variability of overshoot; E) Throughput (left panel) and Calibrated Throughput (right panel); F) shows the linear relationship between completion time (CT) and index of difficulty (ID) and the average completion time in each control strategy; G) shows the force control stability, and the smaller FM_{RMSE}, the higher the stability; H) shows the force similarity (FS) between the force generated by prosthetic hand and the contralateral hand. (*, $p < 0.05$; **, $p < 0.01$; ***, $p < 0.001$).

inertia of bones [48], the closed-loop adjustment of reflex [49], etc.

In the case of prosthesis control, the CNS of amputees is almost intact. What is missing are the neuro-musculo-skeletal system and disrupted efferent and afferent information. Technologies are also rapidly advancing for restoration of tactile sensation (reviewed in [6]), which may transcend the functionality of prosthetic hand [50]. Therefore, the missing neuro-biomechanical properties are the main targets for compensation using the biomimetic controller. The neural interfaces that can detect true motor intensions of amputees would guarantee neural compatibility of the hand prosthesis with CNS [18]. Performance of a normal hand imposes a high standard that might be insurmountable by prosthetic hands. Therefore, the performance gap presents a challenging goal for the biomimetic controller to confront. It is essential to show

and acknowledge the performance gap when establishing the feasibility of biomimetic controller.

Multiple reasons might explain why our biomimetic approach may facilitate the control of grasping force. *First*, the models created an informational context compatible with motor commands decoded from EMG [18]. More specifically, the alpha motor commands originally intended for driving a plant with force-length property, reflex modulation, etc., therefore the biomimetic model provided such a context that may feel natural for the amputee. *Second*, adopting neuromuscular-like properties in the biomimetic controller restores part of the disrupted neuro-mechanical coupling [51]. As a result, when the prosthetic hand interacts with objects, the force applied on the object is likely more stable and less susceptible to sudden changes. *Third,* having muscle spindles in the model may compensate for inaccurate estimations in the feedforward commands [17]. Even though the quasi-static task incurred minimal changes in the length of musculotendonal unit, changes may still occur in the fascicle length, which will be sensed into the closed-loop control by the spindles. In this case, we tend to think the users did not *directly* take advantage of the proprioceptive feedback, but rather they relied on the closed-loop behavior of the biomimetic controller to help with task completion. Since the biomimetic controller continuously processed proprioceptive information, the amputee might eventually benefit from the proprioceptive feedback.

It is noteworthy that for the prosthetic control and human hand control, p-value in Fitts regression in the full-hand experiment was lower than that of the single-finger experiment (Fig. 8F and Fig. 9F). The possible reason was that the target forces in the full-hand task was greater than those in the single-finger task. Incremental increases in muscle force were produced by progressive recruitment of more motor neurons. As muscle force increased, fluctuations in the number of motoneurons might lead to greater fluctuations in force due to motor-dependent noise [52].

One limitation of this study was that the task of "press-without-break" required constant visual feedback, which is not usually the case in daily tasks. In absence of vision, tactile sensation becomes the most critical information for online force control [50], [53]. If tactile and proprioceptive information can be informed to the amputee, the performance of prosthetic control may continue approaching to the level of human hand. Another potential improvement to the existing design is to add an antagonistic muscle in the biomimetic controller. This would require a second EMG signal for control, which might be challenging on amputees, but it would enable a direct manipulation of joint stiffness following human-like reflex mechanisms. Further tests of the biomimetic controller are necessary to demonstrate its functional benefits with real-life grasp tasks in a larger group of amputees. It will also be informative to illustrate full capacity of the biomimetic control system in capturing human-like sensorimotor behaviors.

V. Conclusion

In conclusion, our results presented strong evidence that incorporating neuromuscular reflex properties in the biomimetic controller may enhance motor performance of amputees operating a tendon-driven prosthetic hand. Further studies are required to explore the compliant properties offered by the biomimetic controller and performance benefits arising from neuromuscular reflex.

References

[1] C. M. Niu, Q. Luo, C.-H. Chou, J. Liu, M. Hao, and N. Lan, "Neuromorphic model of reflex for realtime human-like compliant control of prosthetic hand," *Ann. Biomed. Eng.*, vol. 49, no. 2, pp. 673–688, Feb. 2021, doi: 10.1007/s10439-020-02596-9.

[2] L. Resnik *et al.*, "Advanced upper limb prosthetic devices: Implications for upper limb prosthetic rehabilitation," *Arch. Phys. Med. Rehabil.*, vol. 93, no. 4, pp. 710–717, Apr. 2012, doi: 10.1016/j.apmr.2011.11.010.

[3] M. Atzori and H. Müller, "Control capabilities of myoelectric robotic prostheses by hand amputees: A scientific research and market overview," *Frontiers Syst. Neurosci.*, vol. 9, p. 162, Nov. 2015, doi: 10.3389/fnsys.2015.00162.

[4] D. J. Atkins, D. C. Y. Heard, and W. H. Donovan, "Epidemiologic overview of individuals with upper-limb loss and their reported research priorities," *J. Prosthetics Orthotics*, vol. 8, no. 1, pp. 2–11, 1996.

[5] E. A. Biddiss and T. T. Chau, "Upper limb prosthesis use and abandonment: A survey of the last 25 years," *Prosthetics Orthotics Int.*, vol. 31, no. 3, pp. 236–257, Sep. 2007, doi: 10.1080/03093640600994581.

[6] S. J. Bensmaia, D. J. Tyler, and S. Micera, "Restoration of sensory information via bionic hands," *Nature Biomed. Eng.*, pp. 1–13, Nov. 2020, doi: 10.1038/s41551-020-00630-8.

[7] C. L. Taylor and R. J. Schwarz, "The anatomy and mechanics of the human hand," *Artif. Limbs*, vol. 2, no. 2, pp. 22–35, May 1955.

[8] L. A. Jones and S. J. Lederman, *Human Hand Function*. New York, NY, USA: Oxford University Press, 2006.

[9] T. Tsuji, P. G. Morasso, K. Goto, and K. Ito, "Human hand impedance characteristics during maintained posture," *Biol. Cybern.*, vol. 72, no. 6, pp. 475–485, May 1995, doi: 10.1007/BF00199890.

[10] J. R. Napier, "The prehensile movements of the human hand," *J. Bone Joint Surg.*, vol. 38, no. 4, pp. 902–913, Nov. 1956.

[11] R. S. Johansson and G. Westling, "Coordinated isometric muscle commands adequately and erroneously programmed for the weight during lifting task with precision grip," *Exp. Brain Res.*, vol. 71, no. 1, Jun. 1988, doi: 10.1007/BF00247522.

[12] J. K. Salisbury and J. J. Craig, "Articulated hands: Force control and kinematic issues," *Int. J. Robot. Res.*, vol. 1, no. 1, pp. 4–17, Mar. 1982, doi: 10.1177/027836498200100102.

[13] S. B. Godfrey *et al.*, "SoftHand at the CYBATHLON: A user's experience," *J. NeuroEng. Rehabil.*, vol. 14, no. 1, Dec. 2017, Art. no. 124, doi: 10.1186/s12984-017-0334-y.

[14] R. M. Alexander, "Tendon elasticity and muscle function," *Comparative Biochem. Physiol. A, Mol. Integr. Physiol.*, vol. 133, no. 4, pp. 1001–1011, Dec. 2002, doi: 10.1016/S1095-6433(02)00143-5.

[15] J. C. Houk, W. Z. Rymer, and P. E. Crago, "Dependence of dynamic response of spindle receptors on muscle length and velocity," *J. Neurophysiol.*, vol. 46, no. 1, pp. 143–166, Jul. 1981, doi: 10.1152/jn.1981.46.1.143.

[16] C. D. Marsden, P. A. Merton, and H. B. Morton, "Stretch reflex and servo action in a variety of human muscles," *J. Physiol.*, vol. 259, no. 2, pp. 531–560, Jul. 1976, doi: 10.1113/jphysiol.1976.sp011481.

[17] E. J. Perreault, K. Chen, R. D. Trumbower, and G. Lewis, "Interactions with compliant loads alter stretch reflex gains but not intermuscular coordination," *J. Neurophysiol.*, vol. 99, no. 5, pp. 2101–2113, May 2008, doi: 10.1152/jn.01094.2007.

[18] N. Lan, C. M. Niu, M. Hao, C.-H. Chou, and C. Dai, "Achieving neural compatibility with human sensorimotor control in prosthetic and therapeutic devices," *IEEE Trans. Med. Robot. Bionics*, vol. 1, no. 3, pp. 122–134, Aug. 2019, doi: 10.1109/TMRB.2019.2930356.

[19] I. M. Tarkka, "Short and long latency reflexes in human muscles following electrical and mechanical stimulation," *Acta Physiol. Scandinavica Supplementum*, vol. 557, pp. 1–32, Jan. 1986.

[20] S. Li *et al.*, "Coordinated alpha and gamma control of muscles and spindles in movement and posture," *Frontiers Comput. Neurosci.*, vol. 9, p. 122, Oct. 2015, doi: 10.3389/fncom.2015.00122.

[21] X. He, Y.-F. Du, and N. Lan, "Evaluation of feedforward and feedback contributions to hand stiffness and variability in multijoint arm control," *IEEE Trans. Neural Syst. Rehabil. Eng.*, vol. 21, no. 4, pp. 634–647, Jul. 2013, doi: 10.1109/TNSRE.2012.2234479.

[22] C. M. Niu, K. Jalaleddini, W. J. Sohn, J. Rocamora, T. D. Sanger, and F. J. Valero-Cuevas, "Neuromorphic meets neuromechanics, Part I: The methodology and implementation," *J. Neural Eng.*, vol. 14, no. 2, Apr. 2017, Art. no. 025001, doi: 10.1088/1741-2552/aa593c.

[23] N. Lan *et al.*, "Next-generation prosthetic hand: From biomimetic to biorealistic," *Research*, vol. 2021, pp. 1–4, Mar. 2021, doi: 10.34133/2021/4675326.

[24] P. J. Kyberd *et al.*, "MARCUS: A two degree of freedom hand prosthesis with hierarchical grip control," *IEEE Trans. Rehabil. Eng.*, vol. 3, no. 1, pp. 70–76, Mar. 1995, doi: 10.1109/86.372895.

[25] K. Englehart and B. Hudgins, "A robust, real-time control scheme for multifunction myoelectric control," *IEEE Trans. Biomed. Eng.*, vol. 50, no. 7, pp. 848–854, Jul. 2003, doi: 10.1109/TBME.2003.813539.

[26] J. L. Segil, S. A. Huddle, and R. F. F. Weir, "Functional assessment of a myoelectric postural controller and multi-functional prosthetic hand by persons with trans-radial limb loss," *IEEE Trans. Neural Syst. Rehabil. Eng.*, vol. 25, no. 6, pp. 618–627, Jun. 2017, doi: 10.1109/TNSRE.2016.2586846.

[27] L. Schmalfuss *et al.*, "A hybrid auricular control system: Direct, simultaneous, and proportional myoelectric control of two degrees of freedom in prosthetic hands," *J. Neural Eng.*, vol. 15, no. 5, Oct. 2018, Art. no. 056028, doi: 10.1088/1741-2552/aad727.

[28] J. M. Hahne, M. A. Schweisfurth, M. Koppe, and D. Farina, "Simultaneous control of multiple functions of bionic hand prostheses: Performance and robustness in end users," *Sci. Robot.*, vol. 3, no. 19, Jun. 2018, Art. no. eaat3630, doi: 10.1126/scirobotics.aat3630.

[29] K. Z. Zhuang *et al.*, "Shared human–robot proportional control of a dexterous myoelectric prosthesis," *Nature Mach. Intell.*, vol. 1, no. 9, pp. 400–411, Sep. 2019, doi: 10.1038/s42256-019-0093-5.

[30] Q. Luo, C. M. Niu, and N. Lan, "Effect of fascicle length range on force generation of model-based biomimetic controller for tendon-driven prosthetic hand," presented at the Conf. IEEE Eng. Med. Biol. Soc. (EMBC), Nov. 2021.

[31] T. D. Sanger, "Bayesian filtering of myoelectric signals," *J. Neurophysiol.*, vol. 97, no. 2, pp. 1839–1845, Feb. 2007, doi: 10.1152/jn.00936.2006.

[32] R. Shadmehr and S. P. Wise, *A Mathematical Muscle Model in Supplementary Documents for Computational Neurobiology of Reaching and Pointing*. Cambridge, MA, USA: MIT Press, 2005.

[33] C. S. Cook and M. J. N. McDonagh, "Measurement of muscle and tendon stiffness in man," *Eur. J. Appl. Physiol. Occupat. Physiol.*, vol. 72, no. 4, pp. 380–382, 1996, doi: 10.1007/BF00599700.

[34] F. E. Zajac, "Muscle and tendon: Properties, models, scaling, and application to biomechanics and motor control," *Crit. Rev. Biomed. Eng.*, vol. 17, no. 4, pp. 359–411, 1989.

[35] I. E. Brown, T. L. Liinamaa, and G. E. Loeb, "Relationships between range of motion, L_o, and passive force in five strap-like muscles of the feline hind limb," *J. Morphol.*, vol. 230, no. 1, pp. 69–77, Oct. 1996.

[36] A. S. Gailey *et al.*, "Grasp performance of a soft synergy-based prosthetic hand: A pilot study," *IEEE Trans. Neural Syst. Rehabil. Eng.*, vol. 25, no. 12, pp. 2407–2417, Dec. 2017, doi: 10.1109/TNSRE.2017.2737539.

[37] Q. Fu, F. Shao, and M. Santello, "Inter-limb transfer of grasp force perception with closed-loop hand prosthesis," *IEEE Trans. Neural Syst. Rehabil. Eng.*, vol. 27, no. 5, pp. 927–936, May 2019, doi: 10.1109/TNSRE.2019.2911893.

[38] P. M. Fitts, "The information capacity of the human motor system in controlling the amplitude of movement," *J. Exp. Psychol.*, vol. 47, no. 6, pp. 381–391, 1954, doi: 10.1037/h0055392.

[39] P. M. Fitts and J. R. Peterson, "Information capacity of discrete motor responses," *J. Exp. Psychol.*, vol. 67, no. 2, pp. 103–112, Feb. 1964, doi: 10.1037/h0045689.

[40] R. J. Hyndman and A. B. Koehler, "Another look at measures of forecast accuracy," *Int. J. Forecasting*, vol. 22, no. 4, pp. 679–688, Oct. 2006, doi: 10.1016/j.ijforecast.2006.03.001.

[41] H. Liu and M. Schneider, "Similarity measurement of moving object trajectories," in *Proc. 3rd ACM SIGSPATIAL Int. Workshop GeoStreaming (IWGS)*, Redondo Beach, CA, USA, 2012, pp. 19–22, doi: 10.1145/2442968.2442971.

[42] R. H. Baayen, D. J. Davidson, and D. M. Bates, "Mixed-effects modeling with crossed random effects for subjects and items," *J. Memory Lang.*, vol. 59, no. 4, pp. 390–412, Nov. 2008, doi: 10.1016/j.jml.2007.12.005.

[43] H. Quené and H. van den Bergh, "Examples of mixed-effects modeling with crossed random effects and with binomial data," *J. Memory Lang.*, vol. 59, no. 4, pp. 413–425, Nov. 2008, doi: 10.1016/j.jml.2008.02.002.

[44] R. Gentner and J. Classen, "Modular organization of finger movements by the human central nervous system," *Neuron*, vol. 52, no. 4, pp. 731–742, Nov. 2006, doi: 10.1016/j.neuron.2006.09.038.

[45] B. B. Edin, G. Westling, and R. S. Johansson, "Independent control of human finger-tip forces at individual digits during precision lifting," *J. Physiol.*, vol. 450, no. 1, pp. 547–564, May 1992, doi: 10.1113/jphysiol.1992.sp019142.

[46] R. S. Johansson and J. R. Flanagan, "Coding and use of tactile signals from the fingertips in object manipulation tasks," *Nature Rev. Neurosci.*, vol. 10, no. 5, pp. 345–359, May 2009, doi: 10.1038/nrn2621.

[47] F. J. Valero-Cuevas, J. W. Yi, D. Brown, R. V. McNamara, C. Paul, and H. Lipson, "The tendon network of the fingers performs anatomical computation at a macroscopic scale," *IEEE Trans. Biomed. Eng.*, vol. 54, no. 6, pp. 1161–1166, Jun. 2007, doi: 10.1109/TBME.2006.889200.

[48] N. A. Bernstein, *The Co-Ordination and Regulation of Movements*. New York, NY, USA: Pergamon, 1967.

[49] J. Weiler, P. L. Gribble, and J. A. Pruszynski, "Spinal stretch reflexes support efficient hand control," *Nature Neurosci.*, vol. 22, no. 4, pp. 529–533, Apr. 2019, doi: 10.1038/s41593-019-0336-0.

[50] M. Hao *et al.*, "Restoring finger-specific sensory feedback for transradial amputees via non-invasive evoked tactile sensation," *IEEE Open J. Eng. Med. Biol.*, vol. 1, pp. 98–107, 2020, doi: 10.1109/OJEMB.2020.2981566.

[51] P. M. H. Rack and D. R. Westbury, "The effects of length and stimulus rate on tension in the isometric cat soleus muscle," *J. Physiol.*, vol. 204, no. 2, pp. 443–460, Oct. 1969, doi: 10.1113/jphysiol.1969.sp008923.

[52] P. M. Bays and D. M. Wolpert, "Computational principles of sensorimotor control that minimize uncertainty and variability," *J. Physiol.*, vol. 578, no. 2, pp. 387–396, Jan. 2007, doi: 10.1113/jphysiol.2006.120121.

[53] L. Zollo *et al.*, "Restoring tactile sensations via neural interfaces for real-time force-and-slippage closed-loop control of bionic hands," *Sci. Robot.*, vol. 4, no. 27, Feb. 2019, Art. no. eaau9924, doi: 10.1126/scirobotics.aau9924.